Taylor & Francis
Taylor & Francis Group

🔓 OPEN ACCESS

Sensitivity analysis of a scattering-based nonlocal means Despeckling Algorithm

Alessio Di Simone, Gerardo Di Martino, Antonio Iodice and Daniele Riccio

Department of Electrical Engineering and Information Technology, Università degli Studi di Napoli Federico II, Naples, Italy

ABSTRACT

Synthetic Aperture Radar (SAR) images are greatly affected by the speckle noise. In order to improve SAR data readability by human interpreters and information extraction performed by computer programs, a despeckling preprocessing step is mandatory. The authors recently presented a despeckling algorithm based on the a priori knowledge of the local topography. In this paper, an experimental sensitivity analysis of the aforementioned despeckling algorithm is conducted and the main results are discussed. In particular, the sensitivity of the filter against surface parameters and scattering behavior is analyzed. A comprehensive understanding of the role of the Digital Elevation Model resolution and the coregistration step is also provided.

Introduction

Remote sensing data acquired by Synthetic Aperture Radar (SAR) systems represent an essential and useful tool in Earth observation and monitoring, as well as for the study and the analysis of other celestial bodies. However, SAR images are greatly affected by the multiplicative noise, named speckle, typical of coherent acquisition systems, like SAR sensors. Speckle noise significantly degrades the appearance of SAR imagery and affects the performance of both scene analysis and interpretation by SAR expert users and information extraction performed by computer programs. Despeckling is then an essential preprocessing step, since a despeckling algorithm can, at least in principle, dramatically improve SAR data readability and interpretation also for SAR non-expert users.

Starting with the simple spatial multilook approach, numerous techniques and approaches have been developed so far Deledalle et al. (2009), Parrilli et al. (2012), Di Martino et al. (2015), Di Martino et al. (2016), Di Martino et al. (2016a). Most techniques are based on the straightforward idea of averaging similar pixels (or patches, i.e. group of pixels) in order to reduce speckle effects. So far, the most promising techniques can be arguably considered the nonlocal-means-based and wavelet-based approaches Di Martino et al. (2014a), Deledalle et al. (2009), Parrilli et al. (2012). The nonlocal framework introduces a novel and interesting similarity criterion based on statistical concepts rather than geometrical ones. Recently, these

methods have been properly extended to SAR imagery in the Probabilistic Patch-Based (PPB) filter Deledalle et al. (2009). Denoising and despeckling were the most promising and successful applications of signal processing in the wavelet domain. All of these concepts were recently applied in the very promising SAR Block-Matching 3-D (SARBM3D) filter proposed in Parrilli et al. (2012). However, state-of-the-art techniques are essentially based on statistical and/or geometrical concepts and approaches with limited physical insight. Actually, electromagnetic scattering plays a key role in SAR imagery acquisition process, as well as in speckle noise formation. Consequently, a more physical-based approach cannot be set up without explicitly taking into account the electromagnetic phenomenology, i.e. the scattering mechanisms, involved in SAR imagery. The authors recently introduced a novel scattering-based despeckling algorithm Di Martino et al. (2015) and applied scattering concepts to PPB Di Martino et al. (2016) and SARBM3D Di Martino et al. (2016a). It is noticeable that, at least in principle, any despeckling algorithm coping with SAR intensity models could take advantage of scattering issues, inserting physical-based concepts into the filter.

The scattering-based PPB, named SB-PPB in Di Martino et al. (2016), accounts for the scattering behavior of the surface via a proper scattering model suitable for natural surfaces. In particular, the surface backscattering coefficient (or Normalized Radar Cross Section, NRCS) is estimated from the surface topography and inserted within the filter as a kind of a priori

CONTACT Alessio Di Simone ✉ alessio.disimone@unina.it 🖥 Department of Electrical Engineering and Information Technology, Università degli Studi di Napoli Federico II, Via Claudio 21, 80125 Naples, Italy

information. Accordingly, a Digital Elevation Model (DEM) of the considered scene must be available to apply the SB-PPB filter. The scattering-based technique proposed by the authors exhibits better performance w. r.t. the state of the art, both in terms of speckle reduction and details preservation Di Martino et al. (2016).

In this paper, we provide a sensitivity analysis of the SB-PPB filter despeckling capability against four different features of the scene and of the algorithm:

- the scattering model describing the surface;
- surface parameters errors apart from the local incidence angle;
- the DEM resolution;
- errors in the SAR image-DEM coregistration step.

In particular, the paper is organized as follows. In "The PPB filter and its scattering-based version", the original PPB and the proposed scattering-based version (SB-PPB) are briefly described. In "Sensitivity analysis of SB-PPB", the sensitivity analysis is described and the main results are presented and discussed. "Conclusions" concludes the paper with some relevant remarks and future recommendations.

The PPB filter and its scattering-based version

The PPB filter, originally described in Deledalle et al. (2009) is a nonlocal means despeckling filter based on a weighted maximum likelihood estimation approach. Within this nonlocal framework, the estimated backscattering coefficient $\hat{\sigma}_s^{WMLE}$ relevant to pixel s is a weighted average of the intensity A_t^2 relevant to pixel t, with t varying within a window Ω centered in s:

$$\hat{\sigma}_s^{WMLE} = \frac{\sum_{t\in\Omega} w_{s,t} A_t^2}{\sum_{t\in\Omega} w_{s,t}}, \qquad (1)$$

wherein the weight $w_{s,t} \in [0, 1]$, is a decreasing function of the logarithmic distance developed in Deledalle et al. (2009) between the target pixel s and the test pixel t. The search window Ω must be chosen taking into account the trade-off between speckle rejection and computational complexity. The patch concept is introduced in Deledalle et al. (2009) in order to consider the neighborhood of the target pixel, so that the weight $w_{s,t}$ is defined as a proper power of the probability that the two patches Δs and Δt centered in s and t, respectively, share the same distribution parameter, i.e.:

$$w_{s,t}^{(non-it.PPB)} \stackrel{\Delta}{=} p(\sigma_{\Delta s} = \sigma_{\Delta t}|A)^{\frac{1}{h}}, \qquad (2)$$

where h is a filter parameter governing the weight decay and the superscript stands for the noniterative PPB. An iterative scheme is proposed in Deledalle et al. (2009) in order to refine the weights estimation. The weight at iteration i is defined as follows:

$$w_{s,t}^{(it.PPB,i)} \stackrel{\Delta}{=} p(\sigma_{\Delta s} = \sigma_{\Delta t}|A, \hat{\sigma}^{i-1})^{\frac{1}{h}}, \qquad (3)$$

where $\hat{\sigma}^{i-1}$ is the NRCS estimation at iteration i-1.

Via the usual Nagakami–Rayleigh distribution for the pixel amplitude A and the Kullback–Leibler divergence for the a priori information modelization in the iterative scheme, definitions in (2) and (3) read as Deledalle et al. (2009):

$$w_{s,t}^{(non-it.PPB)} = \exp\left[-\sum_k \frac{1}{\tilde{h}}\ln\left(\frac{A_{s,k}}{A_{t,k}} + \frac{A_{t,k}}{A_{s,k}}\right)\right], \quad (4)$$

$$w_{s,t}^{(it.PPB,i)}$$
$$= \exp\left[-\sum_k \left(\frac{1}{\tilde{h}}\ln\left(\frac{A_{s,k}}{A_{t,k}} + \frac{A_{t,k}}{A_{s,k}}\right) + \frac{L}{T_{fil}}\frac{\left|\hat{\sigma}_{s,k}^{i-1} - \hat{\sigma}_{t,k}^{i-1}\right|^2}{\hat{\sigma}_{s,k}^{i-1}\hat{\sigma}_{t,k}^{i-1}}\right)\right], \qquad (5)$$

where L stands for the equivalent number of looks, $\tilde{h} = h/(2L-1)$, and T_{fil} is a filter parameter dictating the decay of the Kullback–Leibler divergence.

Scattering-based PPB

In Di Martino et al. (2016), the authors proposed an adaptive scattering-based version of the PPB filter originally proposed in Deledalle et al. (2009) and named it SB-PPB. The key feature of the SB-PPB filter is the ability to take into account the scattering behavior of the imaged surface. More precisely, by applying the same approach used in Deledalle et al. (2009), the filter weights are defined as

$$w_{s,t}^{SB-PPB\ non-it.} \stackrel{\Delta}{=} p(\sigma_{\Delta s} = \sigma_{\Delta t}|A, \hat{\sigma}^{SPM})^{\frac{1}{h}}, \qquad (6)$$

where the superscript "SB-PPB non-it" stands for the noniterative version of the SB-PPB algorithm, and $\hat{\sigma}^{SPM}$ is the backscattering coefficient estimated via a proper scattering model, as described below. As a consequence, the filter weight reads as Di Martino et al. (2016):

$$w_{s,t}^{SB-PPB\ non-it.}$$
$$= \exp\left[-\sum_k \left(\frac{1}{\tilde{h}}\ln\left(\frac{A_{s,k}}{A_{t,k}} + \frac{A_{t,k}}{A_{s,k}}\right) + \frac{L}{T_{fil}}\frac{\left|\hat{\sigma}_{s,k}^{SPM} - \hat{\sigma}_{t,k}^{SPM}\right|^2}{\hat{\sigma}_{s,k}^{SPM}\hat{\sigma}_{t,k}^{SPM}}\right)\right]$$
$$= w_{s,t}^{PPB\ non-it} \cdot \exp\left(-\sum_k \frac{L}{T_{fil}}\frac{\left|\hat{\sigma}_{s,k}^{SPM} - \hat{\sigma}_{t,k}^{SPM}\right|^2}{\hat{\sigma}_{s,k}^{SPM}\hat{\sigma}_{t,k}^{SPM}}\right). \qquad (7)$$

for the noniterative version of the filter. The scattering behavior of the surface is described by its backscattering coefficient $\hat{\sigma}^{SPM}$, that is estimated assuming the knowledge of the surface topography. In particular, within the framework proposed in Di Martino et al. (2016), the surface roughness is modeled as a (topological) 2-D fractional Brownian motion (fBm) stochastic process. For what concerns the scattering

behavior of the considered surfaces, it is noteworthy that the surfaces of interest within the SB-PPB filter, namely, the bare soil natural ones, are predominantly characterized by single bounce scattering phenomena, i.e. no volume scattering and/or multiple bounce phenomena occur. In Di Martino et al. (2016), single bounce phenomena are described via the small perturbation method (SPM) suitable for fractal surfaces:

$$\sigma_{mn}^{SPM} = 2\pi 8\kappa^4 S_0 |\beta_{mn}|^2 \frac{\cos^4\vartheta}{(2k\sin\vartheta)^{2+2H}}, \qquad (8)$$

wherein σ_{mn}^{SPM} is the monostatic NRCS, m and n denote the transmitted and received polarizations, respectively, κ is the electromagnetic wavenumber of the incident field; S_0 is a parameter characterizing the spectral behavior of the physical fBm surface, expressed in $[m^{-2-2H}]$, and related to the fractal parameters T (standing for the topothesy of the surface) and H (standing for the Hurst coefficient of the surface and varying in the range $[0, 1]$); β_{mn}, accounting for the incident and reflected fields polarization, is a function of both the complex relative dielectric constant ε_r of the surface and the local incidence angle ϑ Franceschetti and Riccio (2007).

As shown in the Appendix in Di Martino et al. (2016), the huge number of parameters influencing the signal backscattered from the surface does not prevent a satisfactory (for the speckle filtering purposes) estimation of the a priori scattering information in eq. (8), that can be provided once the knowledge of the most influencing parameter (i.e. the local incidence angle) is assumed. According to this approach, in Di Martino et al. (2016), a DEM of the sensed surface is exploited to compute the local incidence angle map needed for the NRCS estimation.

In order to retain the edge preservation capability of the original PPB filter, an adaptive iterative scheme is proposed in Di Martino et al. (2016). The adaptive scheme is aimed at performing iterations only in flat regions, where non-topography-related SAR intensity variations can be present. In particular, in the first iteration eq. (7) is used, whereas in the subsequent iterations eq. (5) is employed.

Since a detailed description of both the PPB and SB-PPB filters goes outside the main aim of this paper, the reader is referred to Deledalle et al. (2009) and Di Martino et al. (2016) for more details.

Sensitivity analysis of SB-PPB

In this section, a comprehensive sensitivity analysis of the SB-PPB filter is experimentally conducted and the main results are presented and discussed. Following the approach in Di Simone (2016), firstly, different scattering models are used to simulate a set of SAR images in order to qualitatively and quantitatively evaluate the sensitivity of the proposed SB-PPB algorithm against the scattering behavior of the surface. The influence of the surface parameters on the filter performance is then quantitatively evaluated. To this aim, the SB-PPB algorithm is applied to a SAR image using different values for both the electromagnetic and geometrical parameters. The role of the spatial resolution of the DEM is assessed and evaluated by applying the algorithm with different resolution DEMs. Finally, the role of coregistration errors between the DEM and the SAR image is investigated for different DEM resolutions.

For the entire dataset, the underlying topography is simulated via the 2-D fBm surface of fractal parameters $H = 0.8$ and $T = 10^{-5}$m and electromagnetic parameters $\varepsilon_r = 4$ and $\sigma = 10^{-2}$S/m shown in Figure 1(a), while in Figure 1(b) the corresponding local incidence angle map is depicted. Otherwise stated, all the surface parameters, namely, ϑ, H, T, ε_r, and σ are assumed to be known in the SB-PPB filter. For SAR images simulation, the SAR Advanced Simulators (SARAS) simulator described in Franceschetti et al. (1992) is used with the COSMO-SkyMed sensor parameters COSMO-SkyMed System Description & User Guide (2007). The scattering behavior of the surface is simulated via the SPM option of SARAS, unless otherwise stated. The simulated single-look SAR image corresponding to the DEM in Figure 1(a) is displayed in Figure 1(c). The despeckling capabilities of the filter are quantitatively evaluated computing both full-reference and no-reference proper synthetic performance parameters. In particular, the signal-to-noise ratio (SNR), the variance of ratio (VoR), the coefficient of variation (C_x) and the mean structural similarity index measure (MSSIM) are evaluated, as described in Di Martino et al. (2014a) and Wang et al. (2004). For what concerns SNR and MSSIM, the graphs reported in the following show both the absolute value and the relative value normalized to the maximum. For full-reference measures computation, reference (i.e. speckle-free) SAR images are simulated by incoherently averaging 512 single-look sample images. In order to quantitatively establish the quality of the despeckling algorithm, the reader is referred to the reference image measures in Table 1. The reference image corresponding to the DEM in Figure 1(a) and to the SAR image in Figure 1(c) is displayed in Figure 1(d). The image obtained by using the SB-PPB filter is shown in Figure 1(e). For a better understanding of the key role of the a priori scattering information, comparison with the original PPB filter with four iterations is also provided in Figure 1(f). The T_{fil} parameter of SB-PPB and the corresponding parameter of PPB (named T in the original paper Deledalle et al. (2009) have been optimized in terms of SNR for the SAR image in Figure 1(c). In particular, T_{fil} equals 0.31 and 0.06 in SB-PPB and PPB respectively.
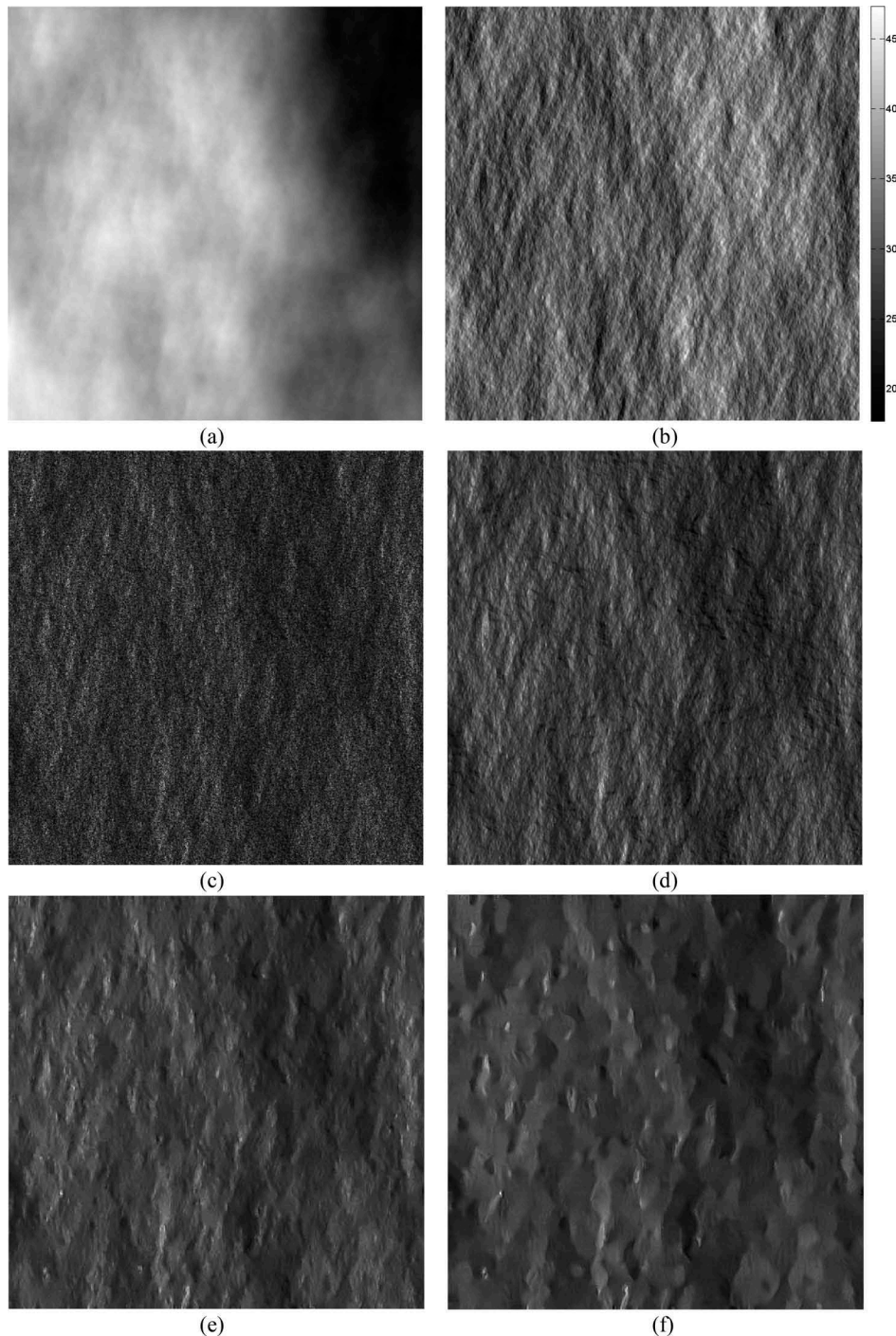
Figure 1. (a) Fractal DEM with fractal parameters $H = 0.8$, $T = 10^{-5}$ m in the azimuth-slant range coordinate system; resolution is 2.58 m and 2.29 m in azimuth and slant-range respectively; (b) local incidence angle map in the azimuth-slant range coordinate system; (c) 512×512 single-look SAR image corresponding to the DEM in (a) and to the electromagnetic parameters $\varepsilon_r = 4$ and $\sigma = 10^{-2}$ S/m; (d) reference image obtained by averaging 512 single-look sample images; (e) SB-PPB with a priori scattering information estimated from (b) and assuming the right values for the surface parameters; (f) PPB with four iterations.

Sensitivity against the scattering behavior of the surface

The huge and well-assessed literature about electromagnetic scattering theory provides numerous models for scattering from surfaces, such as the integral equation method,SPM, physical optics, geometrical optics, Kirchhoff approximation, generalized Lambertian law (GLL). For more details the reader is referred to Franceschetti and Riccio (2007), Tsang et al. (2000), Ulaby et al. (1981), Fung et al. (1992), Beckmann and Spizzichino (1987). It is noteworthy that performance of the SB-PPB filter depends on the actual scattering behavior of the surface. In order to assess the robustness of the SB-PPB against the surface scattering mechanisms, we applied the filter to different SAR images of the same surface simulated assuming different scattering models. In particular, besides the SPM model assumed in the theoretical development of the filter Di Martino et al. (2016), the

Table 1. Performance parameters for various scattering models.

	SB-PPB				PPB				Reference			
	SNR	VoR	C_x	MSSIM	SNR	VoR	C_x	MSSIM	SNR	VoR	C_x	MSSIM
SPM	5.669	0.775	0.571	0.996	3.473	0.945	0.511	0.993	∞	0.98	0.67	1
$\cos\vartheta$	−0.084	0.751	0.179	0.999	0.679	0.844	0.122	0.999	∞	1.01	0.15	1
$\cos^2\vartheta$	1.173	0.760	0.201	0.999	1.291	0.865	0.139	0.998	∞	1.02	0.21	1
$\cos^4\vartheta$	2.903	0.758	0.248	0.999	1.981	0.872	0.182	0.998	∞	1.01	0.26	1

$\cos\theta, \cos^2\theta$ and $\cos^4\theta$ GLL scattering models are used for simulation purposes. Results are depicted in Figures 1–4 while the synthetic performance parameters are presented in Table 1. Coherently with the theoretical framework developed in Di Martino et al. (2016), the most accurate results are obtained if the scattering behavior of the surface is correctly described by the SPM model (Figure 1(e)–(f)). If not the case, the more isotropic the scattering, the worse the results. For the considered scattering models, the worst results in terms of SNR are provided with the $\cos\vartheta$ scattering model, while with the $\cos^2\vartheta$ and $\cos^4\vartheta$ models intermediate results are obtained. The poor performance in the $\cos\vartheta$ case in terms of SNR can be partially due to the inadequacy of the Lambertian model to describe the scattering mechanisms at microwaves frequencies Bors et al. (2003), Ruello et al. (2006), Di Martino et al. (2014), Franceschetti and Riccio (2007). In order to improve performance, a suitable value for the T_{fil} parameter is needed, due to its link with the scattering distance decay. This is confirmed by the performance of the PPB filter, whose despeckling capabilities depend on the used scattering model also. However, a good texture preservation is provided by the SB-PPB algorithm whatever the scattering model, as witnessed by the coefficient of variation in Table 1.

Sensitivity against the surface parameters

The SPM model proposed in Di Martino et al. (2016), suitable for bare soil natural surfaces, properly accounts for both electromagnetic and geometrical characteristics of the surface Franceschetti and Riccio (2007). As a consequence, the estimation of the a priori scattering information (see eq. (8)) requires, at least in principle, the knowledge (or estimation) of numerous parameters, namely the local incidence angle ϑ, the Hurst coefficient H, the topothesy T, the relative dielectric constant ε_r, and the electrical conductivity σ. It is noteworthy that an accurate knowledge of all these parameters is not available, at least where SAR data are of interest. However, as demonstrated in Di Martino et al. (2016), a scattering-based approach for the despeckling problem is still applicable since the scattering
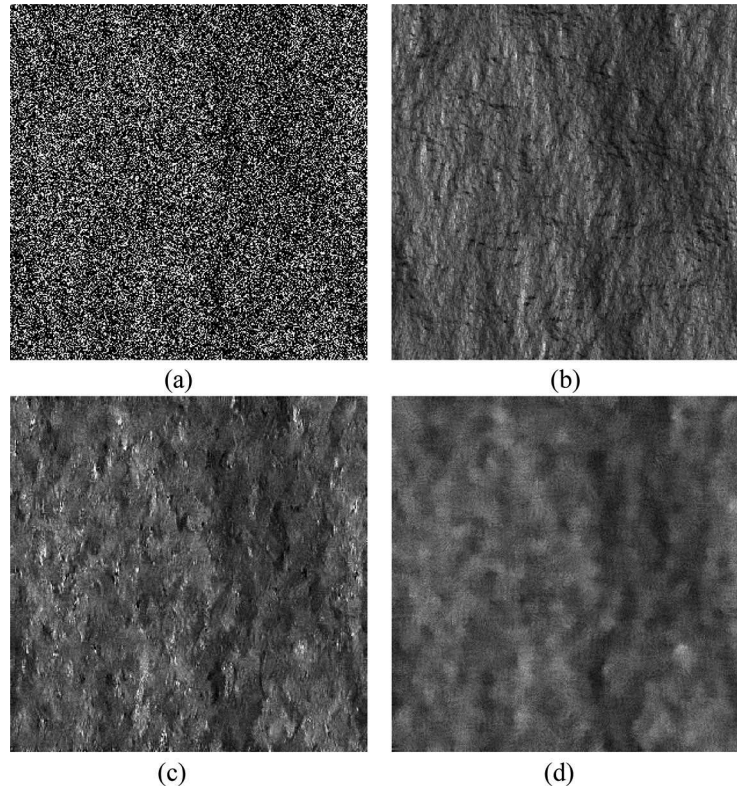
Figure 2. Simulated and despeckled SAR images relevant to the DEM in Figure 1(a) and assuming the $\cos^2\vartheta$ scattering model. (a) Noisy; (b) reference SAR image; (c) SB-PPB; (d) PPB.
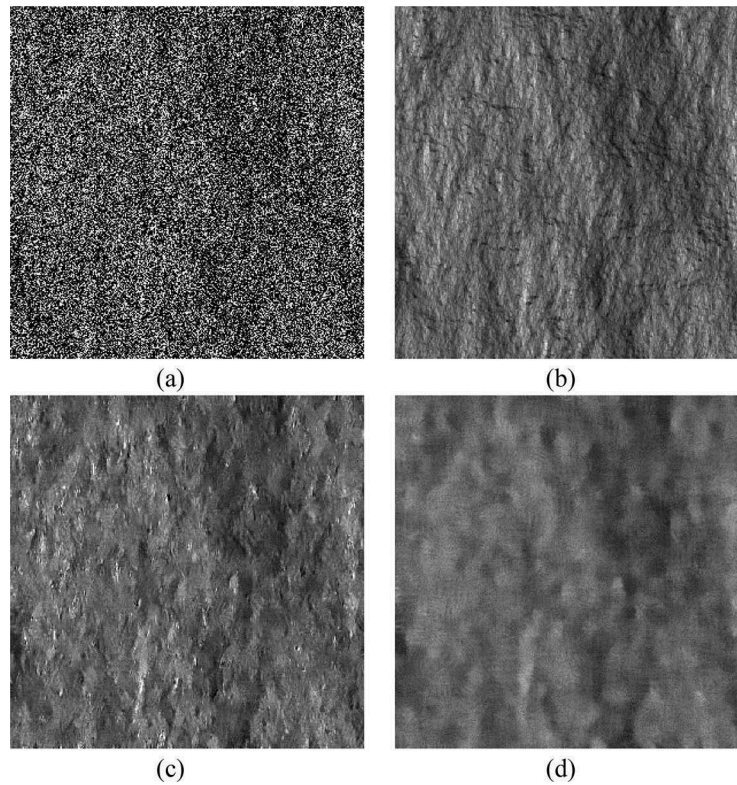
Figure 3. Simulated and despeckled SAR images relevant to the DEM in Figure 1(a) and assuming the $\cos^2 \vartheta$ scattering model. (a) Noisy; (b) reference SAR image; (c) SB-PPB; (d) PPB.

mechanisms do not exhibit the same sensitivity to the different surface parameters. In particular, the sensitivity analysis conducted in Di Martino et al. (2016) shows that the local incidence angle has the major influence on the energy backscattered from the surface, while the remaining parameters represent a minor contribution. Consequently, a reliable estimation of the a priori scattering information is still possible by assuming the availability of the local incidence angle map, i.e. a DEM of the underlying topography is required. For what concerns the remaining parameters, typical values for most bare soil surfaces are used. However, the SB-PPB algorithm is able to take into account the knowledge of whatever surface parameter. For example, in Di Martino et al. (2012), a method for the retrieval of the Hurst coefficient from a single-look SAR image is described; in Iodice et al. (2011) a method to retrieve the soil surface parameters from polarimetric SAR data is presented; in Franceschetti et al. (2000), a general framework for surface parameters estimation from backscattered data is discussed.

In this section, we experimentally assess the robustness of the SB-PPB algorithm with respect to errors in the surface parameters, namely the Hurst coefficient, the relative dielectric constant, and the conductivity, while an accurate knowledge of the local incidence angle is assumed for the a priori scattering information estimation. It is noteworthy that, despite the influence on the backscattering coefficient, the topothesy simplifies in the filter weight evaluation Di Martino et al.

(2016). Consequently, a sensitivity analysis against the topothesy is not conducted. To evaluate the sensitivity of SB-PPB against inaccuracy in the Hurst coefficient, the algorithm is applied to the single-look SAR image in Figure 1(c), relevant to the DEM in Figure 1(a), with different values of the input parameter H. In particular, values within the range [0, 1] are assigned to the latter parameter. The performance parameters of the despeckled image against H depicted in Figure 5 show a nonnegligible influence of the Hurst coefficient on the filter performance thus confirming its nonnegligible influence on the backscattered energy from the surface Di Martino et al. (2016). In particular, in this scenario, a performance degradation up to 20% is experienced in correspondence of very gross errors on H estimation. However, with values of H typical of actual natural surfaces ($0.6 \le H \le 0.9$) Ruello et al. (2006), a considerably smaller degradation (up to 2%) is experienced. Best performance in terms of SNR are ensured with $H = 0.8$, i.e. if an accurate knowledge/estimation of H is available. High H values provide less smoothing and a better texture preservation, as witnessed by the VoR and the C_x parameters. Thus, the higher H, the stronger the decay of the scattering distance. It is noticeable that the nonnegligible influence of the H parameter can be faced via a proper estimation procedure, such as that suitable for single-look SAR data proposed in Di Martino et al. (2012) and actually used in SB-PPB. However, thanks to the a priori scattering information, the SB-PPB provides better results w.r.t. the original PPB for every value of H (performance parameters of PPB are reported in the
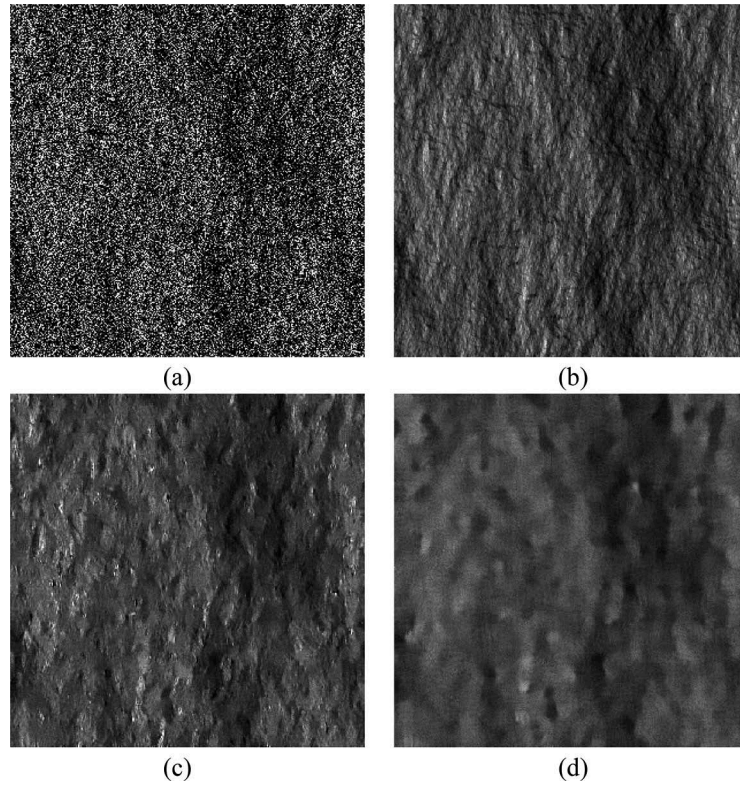
Figure 4. Simulated and despeckled SAR images relevant to the DEM in Figure 1(a) and assuming the $\cos^2 \vartheta$ scattering model. (a) Noisy; (b) reference SAR image; (c) SB-PPB; (d) PPB.
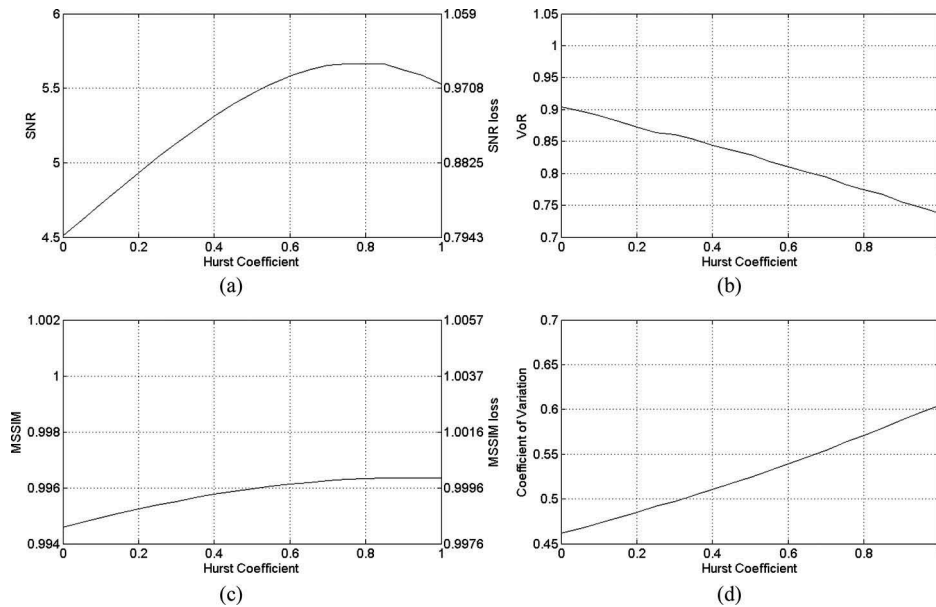
Figure 5. Sensitivity of SB-PPB against the Hurst Coefficient: (a) SNR; (b) VoR; (c) MSSIM; (d) Coefficient of Variation.

SPM row in Table 1). Figures 6 and 7 show the sensitivity of SB-PPB against the relative dielectric constant and the electrical conductivity, respectively. Due to their minor contribution to the backscattered energy, the SB-PPB exhibits robustness against the electromagnetic parameters. The exact knowledge of their value allows a negligible performance improvement. For such parameters, reference values can be used without incurring in a significant performance degradation. For example, typical values for dry soil and damp soil are

$\varepsilon_r = 4$, $\sigma = 10^{-2} \text{S/m}$ and $\varepsilon_r = 10$, $\sigma = 10^{-3} \text{S/m}$, respectively. This allows the applicability of the algorithm even if an estimation/knowledge of the electromagnetic parameters is not available.

Sensitivity against the DEM resolution

In this section, the robustness of SB-PPB against the DEM spatial resolution is analyzed by applying the algorithm to the single-look SAR image depicted in
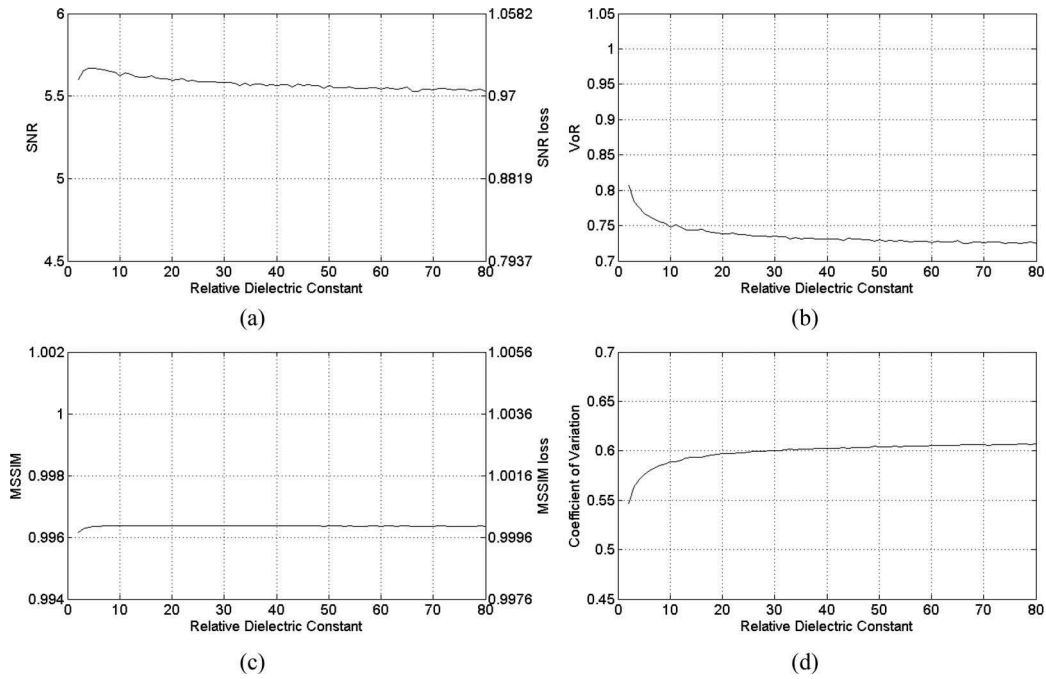
Figure 6. Sensitivity of SB-PPB against the relative dielectric constant: (a) SNR; (b) VoR; (c) MSSIM; (d) Coefficient of Variation.
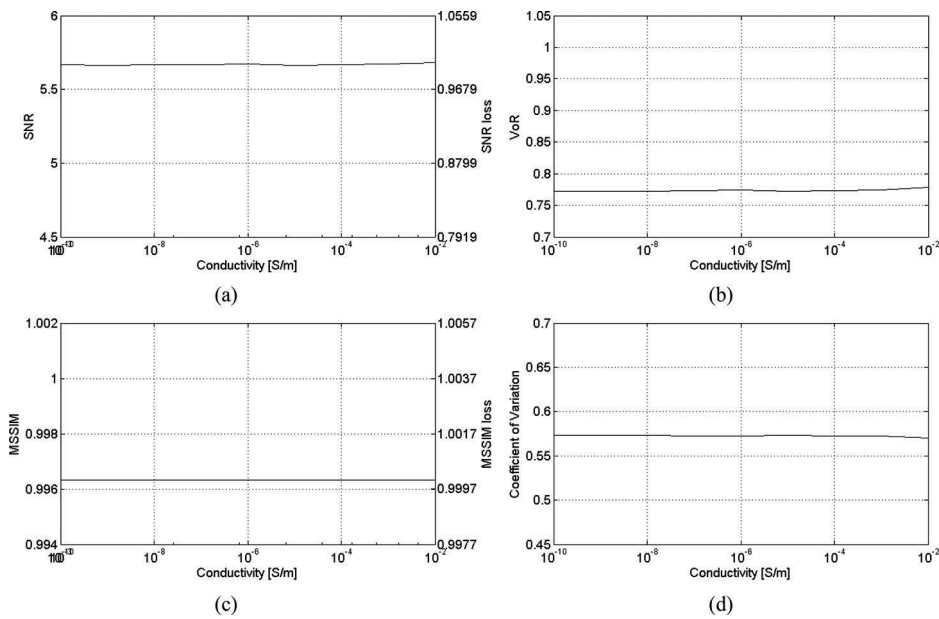
Figure 7. Sensitivity of SB-PPB against the electrical conductivity: (a) SNR; (b) VoR; (c) MSSIM; (d) Coefficient of Variation.

Figure 1(c) with the scattering information evaluated from DEMs with different resolutions. The highest-resolution DEM used (Figure 1(a)) shares the same spatial resolution of the simulated SAR image in Figure 1(c), i.e. 2.58 m in azimuth and 2.29 m in slant range. DEMs with very high-resolution up to 1 m are provided by the more and more diffuse Lidar systems. The spatial resolution of the DEM in Figure 1(a) is then reduced with an increasing power of two up to 512, which corresponds to a spatial resolution of about 1300 m in azimuth and 1170 m in slant range. A gross DEM with similar resolution values is that provided by the Global 30 Arc-Second Elevation (GTOPO30) DEM

[GTOPO30]. The highest-resolution DEM ensures the best performance as shown in Figure 9, providing a SNR improvement of more than 60% of the original PPB. A high-resolution DEM allows a significant speckle rejection without losing fine details, thanks to the richly detailed a priori scattering information. Lowering the resolution of the DEM causes a smoother a priori scattering information, as well as a smoother despeckled image, and a significant detail loss is visible with the lowest resolutions (Figure 8), as witnessed by the high VoR. It is noticeable that with sufficiently low resolution, the a priori scattering information provides worse results than the homogeneous a priori information exploited in the original
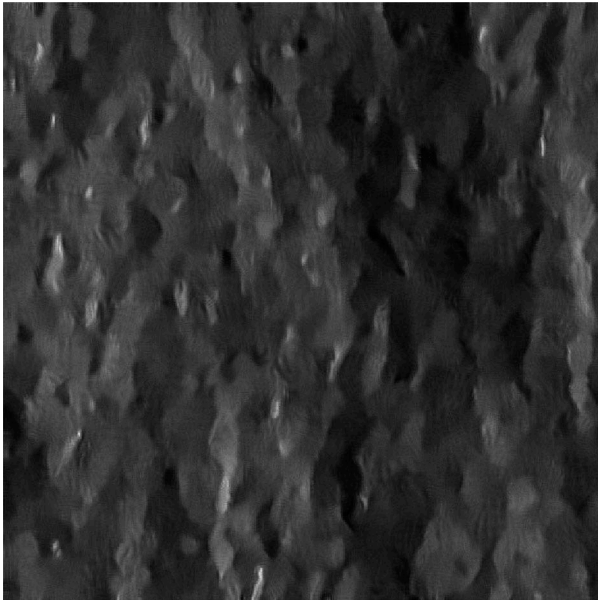
Figure 8. SB-PPB with a priori scattering information estimated from the local incidence angle map in Figure 1(b) filtered with a 512x512 moving average filter and assuming the right values for the surface parameters.

PPB. In particular, with a resolution loss greater than 16, corresponding to a resolution of about 40 m in azimuth and 35 m in slant range, the SB-PPB provides an overall worse result than PPB. With a further increasing of the resolution loss, the a priori scattering information becomes more and more homogeneous; consequently, SB-PPB tends to PPB.

Sensitivity against the DEM coregistration

In this latter section, we evaluate the sensitivity of the SB-PPB algorithm against coregistration accuracy

between the DEM and the SAR image. In order to provide a better understanding of the role of this preprocessing step in the SB-PPB procedure, the robustness is evaluated for different DEM resolutions. Although possible coregistration errors can occur both in azimuth and range directions, in this work, for the sake of simplicity, we consider only errors along the range axis. Similar comments apply to (translation/rotation) errors in other directions. For any fixed DEM resolution, coregistration errors are simulated via an increasing displacement of the local incidence angle map in Figure 1(b) with respect to the SAR image in Figure 1(c). The performance parameters are plotted in Figure 10 where the coregistration errors are in pixels. The figure confirms the relationship between the performance degradation due to coregistration errors and the resolution of the DEM of the underlying topography. In particular, the lower the DEM resolution, the stronger the robustness of SB-PPB against coregistration displacements. Consequently, with high-resolution DEMs, better performance is provided at the cost of a precise coregistration step. If a significant coregistration error occurs, a nonnegligible performance degradation is experienced. On the contrary, low-resolution DEMs provide a worse performance on average, but a more stable one also in presence of a significant displacement between the local incidence angle map and the SAR image. Furthermore, the more significant the high-frequencey content of the surface topography, the greater the sensitivity of the SB-PPB algorithm against coregistration mismatches. The key role of the DEM resolution in the sensitivity of SB-PPB against coregistration mismatches is due to the fact that low-resolution a priori scattering
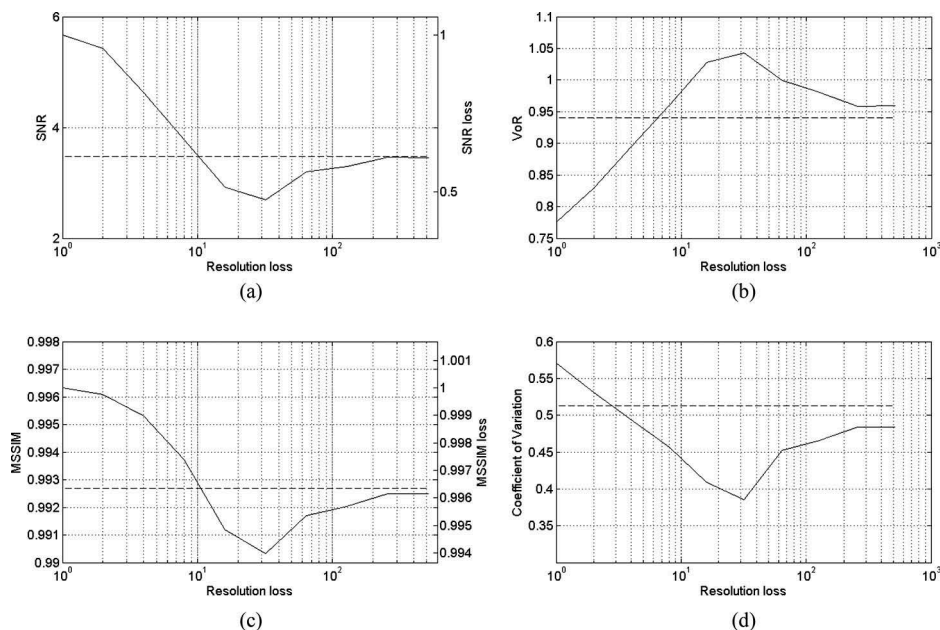
Figure 9. Sensitivity of SB-PPB against the DEM resolution loss: (a) SNR; (b) VoR; (c) MSSIM; (d) Coefficient of Variation. The highest resolution ensures the best performance; with very low-resolution DEMs, SB-PPB tends to PPB (dashed lines).
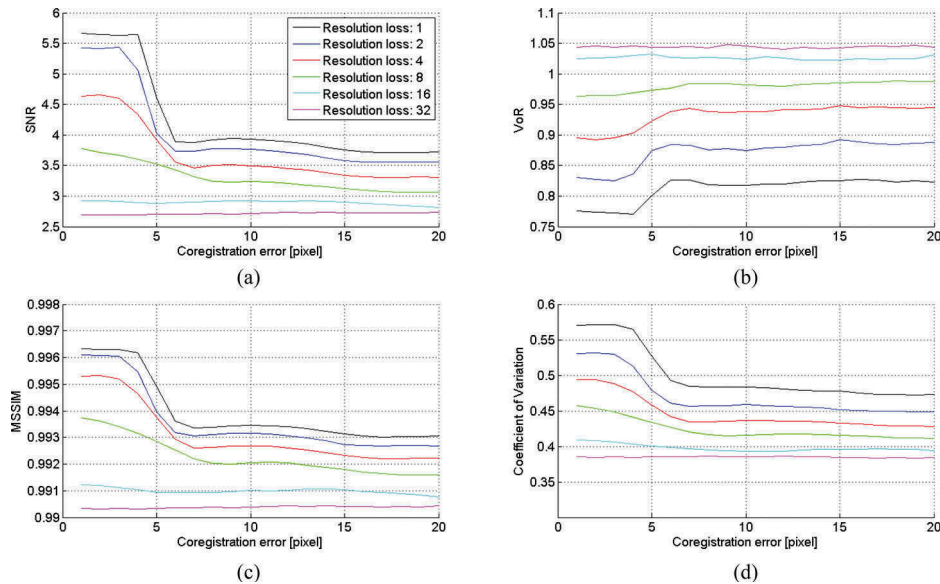
Figure 10. Sensitivity of SB-PPB against coregistration errors (in pixels) between the local incidence angle map and the SAR image for different DEM resolutions. (a) SNR; (b) VoR; (c) MSSIM; (d) Coefficient of Variation. Low-resolution DEMs provide smooth a priori scattering information. Consequently, the lower the DEM resolution, the stronger the sensitivity of SB-PPB against coregistration displacements.

information exhibits less sensitivity against coregistration displacements. Indeed, an homogeneous a priori information is invariant to translation. As shown in Figure 10, in presence of a sufficiently high displacement, a high-resolution DEM may provide worse despeckling capabilities than a low-resolution one. However, for a fixed mismatch, the higher the DEM resolution, the better the despeckling performance. In conclusion, the highest-resolution DEM should be used, unless robustness of the filter is of interest. In the latter case, some smoothing of the DEM can be useful to provide less sensitivity against coregistration displacements.

Conclusions

In this paper, a sensitivity analysis of the SB-PPB despeckling algorithm, recently proposed by the authors in Di Martino et al. (2016), is experimentally conducted. The a priori scattering information, modeled via the SPM model suitable for natural bare soil surfaces, requires, at least in principle, numerous surface parameters to be known/estimated. Although several retrieval algorithms exist in literature, an accurate knowledge of all the required surface parameters does not sound realistic. However, due the major contribution of the local incidence angle to the backscattered energy, a sufficiently accurate estimation (for the considered purposes) of the a priori scattering information is still possible if a DEM of the underlying topography is available. The analysis conducted in this paper experimentally evaluates the robustness of the SB-PPB algorithm against the accuracy of the a priori scattering information. In

particular, the sensitivity analysis is conducted evaluating the influence of four different features on the filter performance:

- scattering model;
- surface parameters errors apart from the local incidence angle;
- DEM resolution;
- errors in the coregistration step.

Concerning the first issue, different scattering models have been used to simulate the scattering behavior of the surface. Best performance is ensured wherein the scattering behavior of the surface is well described by the SPM model used in the SB-PPB algorithm; in more general terms, the more accurate the SPM model, the better the performance of the filter. However, the SB-PPB filter outperforms the original PPB filter for most scattering behaviors. Despeckling capabilities of SB-PPB could take advantage of a scattering model selection algorithm for a suitable filter parameter-tuning preprocessing step.

Among the surface parameters, the Hurst coefficient has nonnegligible influence on the filter performance, providing a significant performance degradation in the case of gross estimation errors. However, in the analyzed case, SB-PPB provides better results than PPB whatever the estimation error. Indeed, the Hurst coefficient can be estimated via the algorithm proposed in Di Martino et al. (2012). If not the case, a reference value can be used. For values of H typical of actual natural surfaces ($0.6 \leq H \leq 0.9$) Ruello et al. (2006), a negligible performance degradation is experienced. The very minor influence of the electromagnetic surface parameters pointed out in the paper suggests the use of reference values.

The DEM resolution plays a key role in the despeckling capabilities of SB-PPB, especially concerning the detail preservation capability. Good performance is ensured by the highest-resolution DEM, thanks to the very detailed a priori information. With decreasing DEM resolution, a dramatic performance drop is experienced. With very low-resolution DEMs, SB-PPB tends to the original PPB, the a priori scattering information tending to the homogeneous a priori information exploited in the PPB filter. For DEM resolutions up to a few times the SAR image resolution, the a priori scattering information ensures better performance than the homogeneous one. The DEM resolution plays a key role even in the robustness of SB-PPB against coregistration mismatches between the SAR image and the DEM. Thus, a high-resolution DEM, even if providing a richly detailed a priori scattering information, causes a significant performance drop in presence of coregistration errors, unless the topography is gentle enough. On the contrary, low-resolution DEMs allow a higher robustness of the filter performance against errors in the coregistration step, thanks to the smoother a priori information. It is worth noticing that authors are currently studying the feasibility of retrieving the local incidence angle map directly from SAR data. This will avoid the need of such extra information and possible coregistration errors.

References

Beckmann, P., & Spizzichino, A. (1987). *The scattering of electromagnetic waves from rough surfaces*. Norwood, MA: Artech House.

Bors, A.G., Hancock, E.R., & Wilson, R.C. (2003). Terrain analysis using radar shape-from-shading. *IEEE Transactions on Pattern Analysis and Machine Intelligence*, 25(8), 974–992. doi:10.1109/TPAMI.2003.1217602

COSMO-SkyMed System Description & User Guide. (2007). Italian Space Agency (ASI), [Online]. Retrieved from http://www.cosmo-skymed.it/docs/ASI-CSM-ENG-RS-093-A-CSKSysDescriptionAndUserGuide.pdf

Deledalle, C.-A., Denis, L., & Tupin, F. (2009). Iterative weighted maximum likelihood denoising with probabilistic patch-based weights. *IEEE Transactions on Image Processing*, 18(12), 2661–2672. doi:10.1109/TIP.2009.2029593

Di Martino, G., Di Simone, A., Iodice, A., Poggi, G., Riccio, D., & Verdoliva, L. (2016a). Scattering-Based SARBM3D. *IEEE Journal of Selected Topics in Applied Earth Observations and Remote Sensing*, 9(6), 2131–2144. doi:10.1109/JSTARS.2016.2543303

Di Martino, G., Di Simone, A., Iodice, A., & Riccio, D. (2016). Scattering-based non-local means SAR despeckling. *IEEE Transactions on Geoscience and Remote Sensing*, 54(6), 3574–3588. doi:10.1109/TGRS.2016.2520309

Di Martino, G., Di Simone, A., Iodice, A., Riccio, D., & Ruello, G. (2014). On shape from shading and SAR images: An overview and a new perspective. In *Proceedings of the IEEE international geoscience and remote sensing symposium,* Quebec, 1333–1336.

Di Martino, G., Di Simone, A., Iodice, A., Riccio, D., & Ruello, G. (2015). Non-local means SAR despeckling based on scattering. *Proceedings of the IEEE International Geoscience and Remote Sensing Symposium*, Milan, 3172–3174.

Di Martino, G., Poderico, M., Poggi, G., Riccio, D., & Verdoliva, L. (2014a). Benchmarking framework for SAR despeckling. *IEEE Transactions on Geoscience and Remote Sensing*, 52(3), 1596–1615. doi:10.1109/TGRS.2013.2252907

Di Martino, G., Riccio, D., & Zinno, I. (2012). SAR imaging of fractal surfaces. *IEEE Transactions on Geoscience and Remote Sensing*, 50(2), 630–644. doi:10.1109/TGRS.2011.2161997

Di Simone, A. (2016). Sensitivity analysis of the scattering-based SARBM3D despeckling algorithm. *Sensors*, 16(7), 971. doi:10.3390/s16070971

Franceschetti, G., Iodice, A., Maddaluno, S., & Riccio, D. (2000). A fractal-based theoretical framework for retrieval of surface parameters from electromagnetic backscattering data. *IEEE Transactions on Geoscience and Remote Sensing*, 38(2), 641–650. doi:10.1109/36.841994

Franceschetti, G., Migliaccio, M., Riccio, D., & Schirinzi, G. (1992). SARAS: A SAR raw signal simulator. *IEEE Transactions on Geoscience and Remote Sensing*, 30(1), 110–123. doi:10.1109/36.124221

Franceschetti, G., & Riccio, D. (2007). *Scattering, natural surfaces and fractals*. Burlington, MA: Academic.

Fung, A.K., Li, Z., & Chen, K.S. (1992). Backscattering from a randomly rough dielectric surface. *IEEE Transactions on Geoscience and Remote Sensing*, 30(2), 356–369. doi:10.1109/36.134085

Global 30 Arc-Second Elevation (GTOPO30). U.S. Geological Survey (USGS), [Online]. Retrieved from https://lta.cr.usgs.gov/GTOPO30

Iodice, A., Natale, A., & Riccio, D. (2011). Retrieval of soil surface parameters via a polarimetric two-scale model. *IEEE Transactions on Geoscience and Remote Sensing*, 49(7), 2531–2547. doi:10.1109/TGRS.2011.2106792

Parrilli, S., Poderico, M., Angelino, C.V., & Verdoliva, L. (2012). A nonlocal SAR image denoising algorithm based on LLMMSE wavelet shrinkage. *IEEE Transactions on Geoscience and Remote Sensing*, 50(2), 606–616. doi:10.1109/TGRS.2011.2161586

Ruello, G., Iodice, A., Mallorqui, J.J., Riccio, D., Broquetas, A., & Franceschetti, G. (2006). Synthesis, construction and validation of a fractal surface. *IEEE Transactions on Geoscience and Remote Sensing*, 44(6), 1403–1412. doi:10.1109/TGRS.2006.870433

Tsang, L., Kong, J.A., & Ding, K. (2000). *Scattering of electromagnetic waves, theories and applications*. New York: John Wiley.

Ulaby, F.T., Moore, R.K., & Fung, A.K. (1981). *Microwave remote sensing: Active and passive, microwave remote sensing fundamentals and radiometry*. Reading, MA: Addison-Wesley.

Wang, Z., Bovik, A.C., Sheikh, H.R., & Simoncelli, E.P. (2004). Image quality assessment: From error visibility to structural similarity. *IEEE Transactions on Image Processing*, 13(4), 600–612. doi:10.1109/TIP.2003.819861